Efficient and accurate simulations of two-dimensional electronic photon-echo signals: Illustration for a simple model of the Fenna–Matthews–Olson complex

Leah Z. Sharp, Dassia Egorova,[a] and Wolfgang Domcke
Department of Chemistry, Technische Universität München, D-85747 Garching, Germany

Two-dimensional (2D) photon-echo spectra of a single subunit of the Fenna–Matthews–Olson (FMO) bacteriochlorophyll trimer of *Chlorobium tepidum* are simulated, employing the equation-of-motion phase-matching approach (EOM-PMA). We consider a slightly extended version of the previously proposed Frenkel exciton model, which explicitly accounts for exciton coherences in the secular approximation. The study is motivated by a recent experiment reporting long-lived coherent oscillations in 2D transients [Engel *et al.*, Nature **446**, 782 (2007)] and aims primarily at accurate simulations of the spectroscopic signals, with the focus on oscillations of 2D peak intensities with population time. The EOM-PMA accurately accounts for finite pulse durations as well as pulse-overlap effects and does not invoke approximations apart from the weak-field limit for a given material system. The population relaxation parameters of the exciton model are taken from the literature. The effects of various dephasing mechanisms on coherence lifetimes are thoroughly studied. It is found that the experimentally detected multiple frequencies in peak oscillations cannot be reproduced by the employed FMO model, which calls for the development of a more sophisticated exciton model of the FMO complex. © *2010 American Institute of Physics*. [doi:10.1063/1.3268705]

I. INTRODUCTION

Photosynthesis, with a quantum yield exceeding 95%, is an extremely efficient mechanism for the absorption and transfer of solar energy and its conversion to chemical energy.[1] Plants and photosynthetic bacteria use complexes built of pigments and proteins to streamline the transfer of energy from light-harvesting antenna systems, which efficiently capture sunlight, to the reaction center, in which energy is stored for later use in biochemical processes.[2] Characteristically, the pigments form a system of electronically coupled excitons,[3] in which the excitation extends over several molecules simultaneously. Thus, the excitation involves several pathways concurrently and selects the most efficient path to the lowest energy state.

The most extensively studied photosynthetic systems are those for which the atomistic structure has been determined by x-ray crystallography, e.g., the peripheral light-harvesting complexes of photosynthetic purple bacteria[4,5] and green plants,[6] as well as the Fenna–Matthews–Olson (FMO) pigment-protein complex of green sulfur bacteria.[7]

First insight into the energy transfer dynamics of the FMO complex was attained from nonlinear ultrafast spectroscopy. Various nonlinear techniques such as hole burning,[8–10] one- and two-color pump probes,[11–17] and accumulated photon-echo (PE) spectroscopy[18] have revealed a number of time scales ranging from 70–100 fs to about 20 ps.

Very recently, two-dimensional (2D) electronic PE spec-tra of the *Chlorobium* (Cb.) *tepidum* FMO complex were recorded.[19,20] In contrast to the previous findings and assumptions, these new experimental results indicate strongly coherent energy-transfer dynamics.[19] The coherent oscillations in the spectroscopic signals were shown to survive on a relatively long time scale of about 700 fs. They were interpreted as a manifestation of electronic coherences, which arise due to the coupling between the excited states of different pigments.[19,20]

The first theoretical models of the FMO complex aimed to reproduce the linear absorption spectrum and the kinetics of the pump-probe spectra.[16,21,22] In these models, the seven pigments of one FMO monomer were treated as seven two-level systems with electronically coupled excited states. The effect of vibrations and protein environment was taken into account by considering the coupling of the electronic degrees of freedom to a phonon bath, which was introduced in a simplified manner; only electronic population relaxation was taken into account and the corresponding relaxation rates were determined by fitting the simulations to the experimental results.

This simple exciton model[22] was also employed for the simulation of 2D spectra.[23] The relaxation rates were computed using a modified Förster/Redfied theory and a reproduction of 2D profiles for finite population times was achieved. However, signatures of coherent energy transfer in 2D signals were out of the scope of these simulations, since coherences between the exciton states were not taken into account. Furthermore, the scheme employed for the simula-

---

a)Electronic mail: egorova@ch.tum.de.

tion of spectra contained a number of crude approximations and, in particular, did not allow for the evaluation of the 2D signal at zero population time.

In contrast to pump-probe experiments, which can be fitted by considering the time evolution of the diagonal elements of the density matrix (populations) only, PE spectroscopy is a coherent technique and knowledge of the time evolution of the off-diagonal elements of the density matrix (coherences) is required for the description of this signal. The first steps toward understanding coherent effects in the 2D spectroscopy of the FMO complex were taken by considering 2D spectra of dimer and trimer systems.[24,25] The simulations showed that electronic coherences can indeed be visualized by the 2D technique as oscillatory beatings of cross peaks in the intensity profiles as a function of the population time. New pulse-sequence schemes have been recently proposed for the investigation of the coherent dynamics of the FMO complex.[26,27] In the reported simulations the off-diagonal elements of the density matrix were taken into account, but their dephasing with population time has been neglected. The signals have been calculated employing doorway-window approximation and a direct comparison with the experiment has not been attempted.

In the present work, we demonstrate the application of the equation-of-motion phase-matching-approach (EOM-PMA)[28–30] for the calculation of 2D electronic PE signals for a Frenkel exciton model. We adopt the model Hamiltonian of the FMO complex as specified in Refs. 22 and 23 and employ an equation of motion, which accounts for the time evolution of populations as well as coherences of the exciton density matrix (within the secular approximation). The electronic population relaxation parameters are taken from Ref. 23, while the pure dephasing rates are considered as adjustable parameters. Given the equation of motion of the material system, the EOM-PMA does not invoke additional approximations apart from the weak-field limit. The comparison of the computed signals with the experimental result thus provides a stringent test of the chosen model of the material dynamics. Very recently, Ishizaki and Fleming[31] employed a dimer model to point out the inadequacy of the standard Redfield equation to treat quantum coherence and long-lived oscillations of 2D peak intensities. This issue is addressed here as well for the Frenkel exciton model of the FMO complex.

It should be stressed that our goal is not the development of an improved model for the description of the photoinduced dynamics of the FMO complex. Rather, we aim at an accurate simulation of 2D PE signals for an existing simple Redfield equation model.[22,23] We systematically study the effects of various dephasing mechanisms on coherence lifetimes. The present work demonstrates the application of the EOM-PMA for the efficient simulation of four-wave-mixing spectra for a reasonably complex material system. Owing to its computational efficiency, the EOM-PMA can be employed for considerably more complex material dynamics featuring, for example, explicit intramonomer or intermonomer electron-vibrational couplings or a nonsecular multilevel Redfield description of vibrational energy and phase relaxation. In fact, the EOM-PMA allows for the simulation of N-wave-mixing signals for any material system for which the equation of motion of the reduced density matrix can be numerically solved for the time scale of interest.[30]

II. COMPUTATIONAL METHODS

A. Model and equation of motion

The FMO pigment-protein complex forms a trimer of identical, weakly interacting subunits. Each monomer contains seven bacteriochlorophyll$a$ (BChl$a$) molecules, which serve to both collect energy and transfer it to the reaction center. The pigments are surrounded by a protein structure that holds the pigments in what are presumably their ideal positions, in order to maximize efficiency, ensure directionality of energy transfer toward the reaction center, and provide an energy sink.[2]

The present study is based on a model of the FMO complex, which has been elaborated over recent years by the analysis of experimental signals such as linear absorption, linear and circular dichroism,[32] pump-probe,[11–17] and 2D PE.[20,23] In this model, the interaction between the subunits is neglected and only a single monomer is considered (a comparative study of the monomer and trimer models justifies this approximation[33]). Each of the seven BChl$a$ molecules within the subunit is represented by an electronic two-level system. The excited states of the molecules are assumed to be coupled to each other and thus form a system of excitons. The vibrational degrees of freedom of the BChl$a$ pigment molecules and the protein environment are taken into account as a thermal bath. The Hamiltonian is thus written as

$$H = H_S + H_B + H_{SB}, \qquad (1)$$

where H_S is the electronic Hamiltonian of the seven BChl$a$ pigment molecules, H_B describes the bath, and H_{SB} determines the sytem-bath interaction. The Hamiltonian H_S can be partitioned into

$$H_S = H_g + H_e, \qquad (2)$$

where H_g and H_e describe the electronic ground states and the excited states of the pigment molecules, respectively. The ground states are assumed to be uncoupled and possess the same ground-state energy, which is set to zero throughout. In the site representation (local basis), H_e reads

$$H_e = \sum_{\alpha=1}^{7} |\alpha\rangle \varepsilon_\alpha \langle\alpha| + \sum_{\alpha \neq \beta} (|\alpha\rangle J_{\alpha\beta}\langle\beta| + |\beta\rangle J_{\beta\alpha}\langle\alpha|), \qquad (3)$$

where $|\alpha\rangle$ denotes the excited states of the BChl$a$ molecules, ε_α are the pertinent vertical excitation energies, and $J_{\alpha\beta}$ are electronic couplings between excited states α and β. The diagonalization of the system Hamiltonian results in the set of seven exciton states $|i\rangle$, with the energies E_i,

$$H_e|i\rangle = E_i|i\rangle. \qquad (4)$$

The parameters of the system Hamiltonian in both the site and the exciton representations were identified from best fits with experimental observables[16,21–23,32] as well as calculated independently.[33,34] The differences in the resulting exciton energies are minor. Here we adopt the set of parameters em-

TABLE I. Site energy levels and electronic couplings (cm^{-1}) of BChl molecules as in the model of Ref. 23.

	BChl 1	BChl 2	BChl 3	BChl 4	BChl 5	BChl 6	BChl 7
BChl 1	12 400	−106	8	−5	6	−8	−4
BChl 2	−106	12 540	28	6	2	13	1
BChl 3	8	28	12 120	−62	−1	−9	17
BChl 4	−5	6	−62	12 295	−70	−19	−57
BChl 5	6	2	−1	−70	12 440	40	−2
BChl 6	−8	13	−9	−19	40	12 480	32
BChl 7	−4	1	17	−57	−2	32	12 380

ployed in Ref. 23, since this set has been used for the calculation of 2D spectra, as in the present work. For the convenience of the reader, we give the parameters in Table I (for ε_α and $J_{\alpha\beta}$) and Table II (for E_i).

A significant effort has been made to characterize the bath (H_B) and the system-bath interaction (H_{SB}) of the model.[23] Further developments have been reported for a dimer system.[31,35] The following simplified equation of motion for the reduced density matrix of a system subject to interaction with a laser field and a dissipative environment is employed ($\hbar=1$):

$$\dot{\rho}(t) = -i[H_S - H_{SF}(t),\rho(t)] - \mathfrak{R}\rho(t), \qquad (5)$$

where ρ is the reduced density matrix of the system, H_{SF} describes the system-field interaction, and the last term, $\mathfrak{R}\rho(t)$, accounts for dissipation. Equation (5) is valid if the system-bath interaction is weak and can be treated perturbatively.

Invoking, furthermore, the secular approximation, the evolution of the diagonal elements of the reduced density matrix is decoupled from the evolution of the off-diagonal elements. According to the Pauli master equation, the dissipation operator for the diagonal elements ("populations") of the system density matrix in the eigenstate (exciton) representation is then

$$\{\mathfrak{R}\rho(t)\}_{ii} = \sum_{j\neq i} (M_{ij}\rho_{ii}(t) - M_{ji}\rho_{jj}(t)). \qquad (6)$$

To describe the relaxation of populations, we adopt the rates M_{ij}, which have been determined in Ref. 23 using a modified Förster/Redfield theory. The dissipation operator for the off-diagonal terms of the reduced density matrix ("coherences") is given by

$$\{\mathfrak{R}\rho(t)\}_{ij} = \xi_{ij}\rho_{ij}(t), \quad \{\mathfrak{R}\rho(t)\}_{ig} = \xi_{ig}\rho_{ig}(t). \qquad (7)$$

The dephasing of the exciton states is determined by ξ_{ij}, whereas the rate of pure optical dephasing between the ground state and the exciton states is denoted by ξ_{ig}. The rates ξ_{ij} can be estimated as $\xi_{ij}=(M_{ij}+M_{ji})/2+\xi_{PD}$, where

ξ_{PD} is the rate of pure dephasing of the exciton states. In this study, ξ_{ij} and ξ_{ig} are treated as adjustable parameters in order to explore their effect on both the coherent dynamics of the system and the 2D signals. Although the relaxation model is oversimplified and cannot account for coherence transfer or memory effects,[31,35] it is sufficient for our purposes: the systematic study of decoherence and population transfer effects on 2D PE spectra within the existing Frenkel exciton model of the FMO complex.

Static disorder, giving rise to inhomogeneous broadening, occurs due to variations in the excited-state transition energy of each molecule. This can be accounted for by using different realizations of the system Hamiltonian to calculate the polarization, and then average over the resulting spectra.[36] In the present work, fluctuations in the transition frequencies are assumed to obey Gaussian distributions of the form

$$\exp(-(E_i' - E_i)^2/2\sigma_i^2), \qquad (8)$$

where the σ_i are the standard deviations, resulting in the full width at half maximum (FWHM) of $2\sqrt{2\ln(2)}\sigma_i$. The broadening of each exciton transition has been previously estimated from the linear absorption spectrum[23] and is given in Table II in terms of FWHM. These data contain both the homogeneous and the inhomogeneous contributions. In order to vary and adjust the strength of the inhomogeneous broadening, we scale the FWHM values of Table II by a factor of $\delta_{inhom} < 1$. The Box–Muller transform has been used to generate normally distributed random numbers.

The system-field interaction in Eq. (5) is defined in the electric-dipole and rotating-wave approximations as

$$H_{SF}(t) = -X\mathbf{E}(t) + H.c. \qquad (9)$$

The electronic transition dipole operator $\hat{\mu}$ of the exciton system is given by the expression

TABLE II. Exciton energy levels (cm^{-1}), dipole strengths ($|\mu_i|^2$), and FWHM (cm^{-1}) of the linear absorption spectrum (Ref. 23).

Exciton	1	2	3	4	5	6	7
E_i	12 101	12 265	12 346	12 397	12 442	12 526	12 600
$|\mu_i|^2$	49	87	73	31	82	24	36
FWHM	141	102	129	123	100	102	129

$$\hat{\mu} = \sum_{i=1}^{7} \mu_i (|g\rangle\langle i| + |i\rangle\langle g|) = X + X^\dagger, \qquad (10)$$

where the μ_i determine the dipole strengths of the excitonic transitions; the values for $|\mu_i|^2$ have been adopted from Ref. 23 and are given in Table II. The three laser pulses that interact with the sample in a PE experiment are characterized by

$$\mathbf{E}(t) = \sum_{a=1}^{3} A e^{-(t-t_a)^2/2\Gamma^2} e^{i\omega t} e^{-i\mathbf{k}_a \mathbf{r}}, \qquad (11)$$

where A, t_a, $\mathbf{k}_a$, and ω are the amplitude, envelope central time, wave vector, and frequency of the pulses. Γ characterizes the pulse duration and is related to the FWHM of the Gaussian pulses as $2\sqrt{2\ln(2)}\Gamma$. Note that all pulses are assumed to have equal amplitudes, carrier frequencies, and durations.

Since the interaction with the laser field, H_{SF}, is included in the commutator in Eq. (5), no *ad hoc* assumption of initial populations is needed. The system is initially in the electronic ground state and the interaction with laser pulses of appropriate duration creates a realistic initial condition.

B. Two-dimensional photon-echo spectroscopy

As in any four-wave mixing scheme, the main computational task is the determination of the induced nonlinear polarization obeying a particular phase-matching condition. Recently, we have proposed an efficient computational scheme, the EOM-PMA,[28–30] which can be implemented to evaluate four-wave mixing signals. The EOM-PMA is valid up to the third order in the system-field interaction. The method has no limitations with respect to pulse duration and automatically accounts for pulse-overlap effects.

The particular realization of the method is determined by the required phase-matching condition. In the case of the PE signal, the system of interest interacts with a series of three laser pulses, which are centered at times t_1, t_2, and t_3, and the phase-matching direction is given by $\mathbf{k}_s = -\mathbf{k}_1 + \mathbf{k}_2 + \mathbf{k}_3$, where $\mathbf{k}_a$ ($a=1,2,3$) denote the wave vectors of the three incoming fields.[37]

In the EOM-PMA, the polarization in the PE direction can be calculated by simultaneously propagating three auxiliary density matrices (σ_1, σ_2, σ_3), each of which obeys a modified equation of motion,[30]

$$\partial_t \sigma_1(t) = -i[H_S - V_1(t,t_1) - V_2^\dagger(t,t_2) - V_3^\dagger(t,t_3), \sigma_1(t)]$$
$$- \Re\sigma_1(t),$$

$$\partial_t \sigma_2(t) = -i[H_S - V_1(t,t_1) - V_2^\dagger(t,t_2), \sigma_2(t)] - \Re\sigma_2(t),$$

$$\partial_t \sigma_3(t) = -i[H_S - V_1(t,t_1) - V_3^\dagger(t,t_3), \sigma_3(t)] - \Re\sigma_3(t),$$
$$(12)$$

where $V_a(t,t_a) = X A e^{-(t-t_a)^2/2\Gamma^2} e^{i\omega t}$. To third order, the desired polarization in the PE direction is then obtained as

$$P_{PE}(t_1,t_2,t_3,t) = e^{i\mathbf{k}_s \cdot \mathbf{r}} \langle X(\sigma_1(t) - \sigma_2(t) - \sigma_3(t)) \rangle + c.c., \qquad (13)$$

where the bracket $\langle \ldots \rangle$ indicates the evaluation of the trace. In this work, the fourth-order Runge–Kutta method with a fixed time step has been used to propagate Eq. (12).

The 2D PE experiment uses the heterodyne detection scheme. In the limit of ideal detection, the heterodyne PE signal is proportional to the polarization $P_{PE}(t_1,t_2,t_3,t)$, where t denotes the detection time. Therefore, the ideally detected 2D spectrum can be calculated as

$$S_{PE}(\omega_\tau, T, \omega_t) \sim \int d\tau \int dt\, e^{-i\omega_\tau \tau} e^{i\omega_t t} P_{PE}(\tau, T, t), \qquad (14)$$

where τ and T denote the delays between the incoming pulses: $\tau = t_2 - t_1$, $T = t_3 - t_2$. The coherence time, τ, corresponds to a period in which the system is in a coherence state after the first interaction with the electric field. The second interaction with the field creates mainly populations, and the delay between the second and the third pulses, T, is therefore referred to as population time. For the case $\tau = 0$, the 2D PE scheme reduces to a frequency-dispersed pump-probe measurement. The population time T is thus analogous to the delay time between pump and probe pulses.

The Fourier transform in Eq. (14) is performed over the coherence time τ and the detection time t. The corresponding frequencies ω_τ, ω_t are often referred to as absorption (or coherence) and emission (or rephasing) frequencies, respectively.

The assumption of a Gaussian envelope for the detection pulse (local oscillator) allows for simulation of realistic detection schemes by postprocessing of spectral data obtained by Eq. (14). To achieve this, the spectra calculated with Eq. (14) are convoluted with a Gaussian function $\exp(-\Gamma^2(\omega_t - \omega)^2/2)$ of the rephasing frequency ω_t to account for the finite duration of the pulse width of physical detectors. The detection pulse is centered at the same wavelength ω as the incoming laser pulses, and its duration has the same FWHM of $2\sqrt{2\ln(2)}\Gamma$. As follows from Eq. (14), the 2D signal is a complex quantity. In the following, only the part associated with the absorptive changes is considered.

The only approximations in the signal calculations of this work are the assumed Gaussian profiles of the field envelopes and the third-order perturbative treatment of the system-field interaction. These assumptions are appropriate for the experiments reported so far. Note, however, that we do not include excited-state absorption (ESA), since our main interest is the detection of coherence survival. ESA is known to influence only the region $\omega_t > \omega_\tau$ of the 2D profiles; our 2D plots do not reproduce the negative contribution due to ESA in this region.

III. RESULTS

In this section, we first briefly discuss the exciton dynamics induced by laser excitation and then turn to simulations of the corresponding 2D spectra. Two electronic 2D PE experiments for the FMO complex have been reported; the pioneering work by Brixner *et al.*,[20] followed more recently

by measurements of Engel *et al.*[19] In Ref. [20], cross peaks indicating couplings between exciton transitions were resolved, and the intensity modulations of the peaks with the population time T were highlighted and analyzed. An additional finding was reported in Ref. [19]. It was demonstrated that both diagonal and cross peaks exhibit coherent oscillations of their intensity with respect to the population time. It has been found that these oscillations survive for at least 660 fs.[19]

Here, we discuss both the overall 2D spectral profiles for various population times as well as intensity modulations of several diagonal and cross peaks as a function of the population time. Therefore, we mainly adopt the work by Engel *et al.*[19] as the experimental reference. The pulse carrier frequencies and durations employed in the calculations are $\omega = 12422$ cm^{-1} (805 nm) and $\Gamma = 17$ fs (40 fs at FWHM), which are very close to the experimental parameters of Ref. [19] (808 nm and 41 fs at FWHM) and Ref. [20] (805 nm and 50 fs at FWHM). The field amplitude is chosen as $A = 40$ cm^{-1} and corresponds to the weak-field regime.

A. Exciton dynamics

Let us first discuss the exciton dynamics, which is initiated by a laser-pulse. The equation of motion, Eq. (5), is solved numerically; H_{SF} represents the interaction with a pump pulse of 40 fs (FWHM) duration and centered at $t=0$. The system is initially in the ground state and the pulse excites all exciton states and creates coherences. Subsequent population dynamics in the exciton representation [diagonal elements $\rho_{ii}(t)$] is shown in Fig. 1(a). The overall population evolution is determined by the master equation, i.e., by the rates M_{ij} and is thus similar to previous reports.[23,33] The initial populations created by the pump pulse are, however, different from those estimated in Ref. [23] (by consideration of the spectral distribution of the laser intensity) and obtained in Ref. [33] [by approximate description of excitation by a pulse of 50 fs (FWHM) duration]. As is seen in the inset in Fig. 1(a), which shows the early time exciton dynamics and the pump-pulse envelope, exciton states two, three and five are populated almost equally and most efficiently. Exciton four is populated to about 44% of the maximum population, while excitons one and seven are each populated to about 37% and exciton six to about 27% of the maximum population. Since the excitation pulse (FWHM 736 cm^{-1}, centered at $\omega = 12422$ cm^{-1}) covers all exciton transitions, the initial populations are primarily determined by the dipole strengths (see Table II). The populations of states four to seven decay much faster than those of the lower exciton states. Around 40 fs, the preparation process is complete and relaxation rates determine the subsequent dynamics. Note that the employed relaxation rates lead to a longer lifetime of exciton three compared to exciton two, even though exciton three has a higher energy.

Figure 1(b) shows the coherence between the excitons 1 and 3, $\rho_{13}(t)$ (this coherence is chosen since it is relevant for the discussion of the 2D spectra below). In the absence of dephasing processes, each coherence oscillates with a frequency determined by the energy difference between the cor-
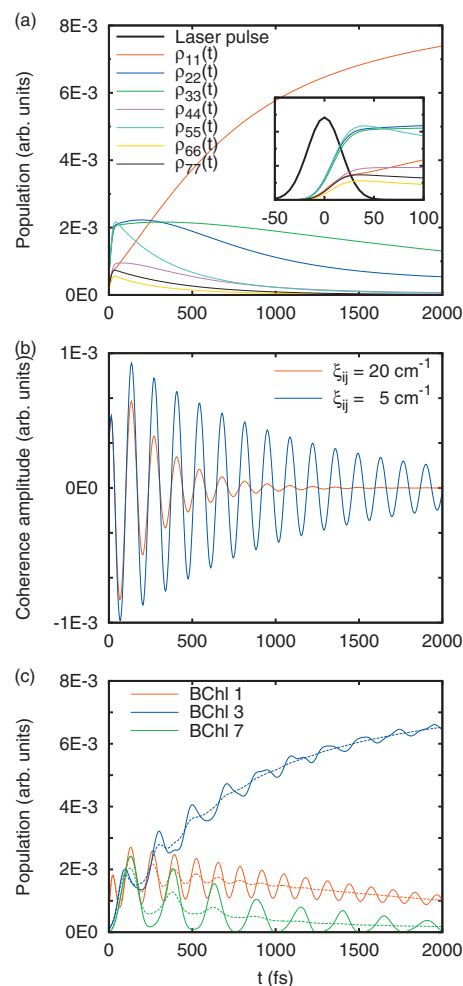

FIG. 1. (a) Electronic population dynamics of the FMO model in terms of the diagonal elements of the density matrix in the exciton representation, $\rho_{ii}(t)$. (b) Off-diagonal element $\rho_{13}(t)$ of the density matrix in the exciton representation (real part) for two dephasing rates, $\xi_{13} = 5$ cm^{-1} (blue line) and $\xi_{13} = 20$ cm^{-1} (red line). (c) Population dynamics of BChl one, three, and seven (site or local representation of the density matrix, $\rho_{\alpha\alpha}(t)$) obtained with $\xi_{ij} = 5$ cm^{-1} (solid lines) and $\xi_{ij} = 20$ cm^{-1} (dashed lines).

responding states; for $\rho_{13}(t)$ the resulting period is 136 fs. Within the present model, the oscillations decay within a time scale dictated by the dephasing rate ξ_{13}. The latter can be estimated as $(M_{13} + M_{31})/2 + \xi_{PD} = 0.6$ ps$^{-1} + \xi_{PD}$. Shown in Fig. 1(b) is $\rho_{13}(t)$ obtained with $\xi_{13} = 5$ cm$^{-1} \approx 0.9$ ps^{-1} (blue line) and $\xi_{13} = 20$ cm$^{-1} \approx 3.7$ ps^{-1} (red line). When $\xi_{13} = 5$ cm^{-1}, the coherences survive for over 2000 fs, while when $\xi_{13} = 20$ cm^{-1}, which is dominated by pure dephasing, the coherences survive for about 1000 fs.

In Fig. 1(c), the population dynamics in the local basis [site representation, $\rho_{\alpha\alpha}(t)$] is shown. The coherence dephasing rates are $\xi_{ij} = 5$ cm^{-1} (solid lines) and 20 cm^{-1} (dashed lines) for all i,j. For clarity, we have picked the excited-state populations of molecules BChl 1 (red lines), BChl 3 (blue lines), and BChl 7 (green lines). The populations of all molecules show pronounced modulations due to exciton coherences that last as long as the coherences survive. The mediating BChl 1 and BChl 7 are seen to be modulated by only one frequency, whereas multiple frequencies contribute to the population dynamics of the BChl 3 excited state. BChl 1, which contributes to excitons three (strongly) and seven
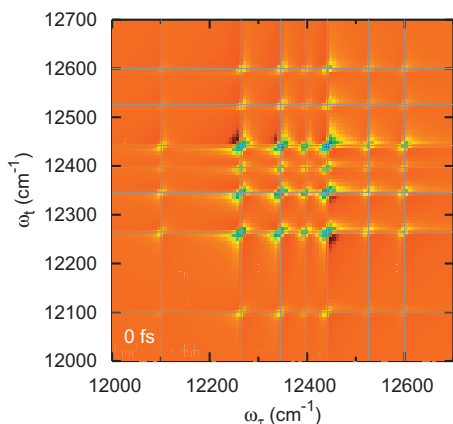
FIG. 2. 2D PE spectra of the FMO model, calculated with a near-ideal value of the optical dephasing rate ($\xi_{ig}=5$ cm^{-1}) and without inhomogeneous broadening ($\delta_{\text{inhom}}=0$) at population time $T=0$. Gray lines are drawn along $w_\tau=E_i$ and $w_t=E_i$ to indicate the locations of exciton transition energies.

(weakly),[23] oscillates with a period of ≈ 131 fs, corresponding to the coherence between excitons three and seven ($\Delta E_{37}=254$ cm^{-1}). Similarly, BChl 7, which contributes to excitons two (weakly) and four (strongly),[23] oscillates with a period of ≈ 255 fs. This corresponds to the coherence between excitons two and four ($\Delta E_{24}=132$ cm^{-1}). The dominating frequency in the BChl 3 dynamics corresponds to the energy difference between excitons one and two ($\Delta E_{12}=164$ cm^{-1}, period of ≈ 200 fs). Note that even a relatively strong exciton dephasing $\xi_{ij}=20$ cm^{-1} gives rise to pronounced coherent modulations of the local populations at times up to ≈ 1000 fs. The picture is very different if the exciton coherences are neglected (see, e.g., the supplementary material of Ref. 34).

B. Two-dimensional spectra

In addition to the relaxation and dephasing parameters relevant to exciton dynamics, the spectroscopic signals are also strongly influenced by optical dephasing and inhomogeneous broadening. In this section, we calculate 2D signals of the model for various population times and address in some

detail the influence of dephasing processes on 2D profiles. Unless otherwise specified, a weak dephasing rate of the exciton coherences is assumed ($\xi_{ij}=5$ cm^{-1}).

We start the discussion in this section by considering a 2D PE spectrum for population time $T=0$ for an idealized case of very weak optical dephasing ($\xi_{ig}=5$ cm^{-1} for all i, which is one order of magnitude less than the average energy difference between successive excitons, 84 cm^{-1}) and no inhomogeneous broadening. Figure 2 shows a very clear pattern in this near-ideal regime. The spectrum exhibits seven characteristic diagonal peaks arising from the transitions to the seven exciton states. The cross peaks, which reflect the couplings between these transitions (via the common ground state), are also observed at their expected positions. The intensity of the peaks is determined by the dipole strengths of the corresponding transitions and slightly modified due to the finite pulse durations [the pulses are centered at 12422 cm^{-1} and have a width (FWHM) of about 736 cm^{-1}]. The effect of ESA is neglected in our calculations. Therefore, the spectral intensity above and below the diagonal is expected to be very similar for population time $T=0$.

The experimental peak profiles of Ref. 19 are significantly broader than the spectrum in Fig. 2 and the individual peaks are not resolved. This suggests that a realistic optical dephasing (homogeneous broadening) is considerably stronger than the employed, $\xi_{ig}=5$ cm^{-1}, and that inhomogeneous averaging must also be taken into account. We first consider the influence of these two broadening mechanisms separately, then study their combined effect.

The spectra shown in Fig. 3 were calculated using optical dephasing rates $\xi_{ig}=20$ cm^{-1} (left panel) and $\xi_{ig}=35$ cm^{-1} (right panel), but without inhomogeneous broadening, $\delta_{\text{inhom}}=0$ (population time $T=0$). As expected, larger values of the dephasing rate lead to broader peaks along both the ω_τ and the ω_t axes. However, in both cases, the peaks are still too localized to be considered accurate reproductions of experimental spectra.[19]

In Fig. 4, inhomogeneous broadening is included, while the optical dephasing rate is kept at 5 cm^{-1}. Shown are the signals at $T=0$ for $\delta_{\text{inhom}}=0.5$ (left panel) and $\delta_{\text{inhom}}=0.7$
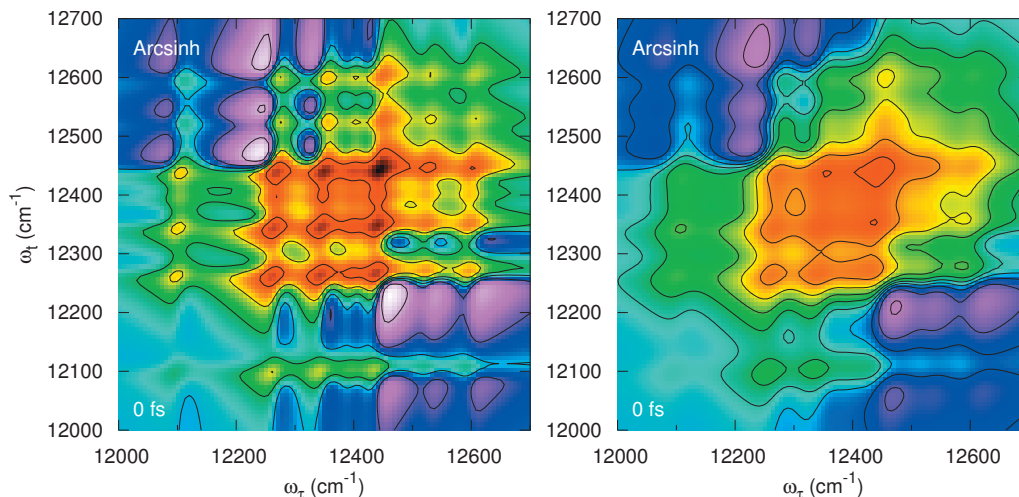

FIG. 3. 2D PE spectra of the FMO model obtained with an optical dephasing rate of $\xi_{ig}=20$ cm^{-1} (left panel) and $\xi_{ig}=35$ cm^{-1} (right panel) for population time $T=0$, in the absence of inhomogeneous broadening. The spectra are displayed with arcsinh scaling to enhance weaker aspects of the peak profiles.
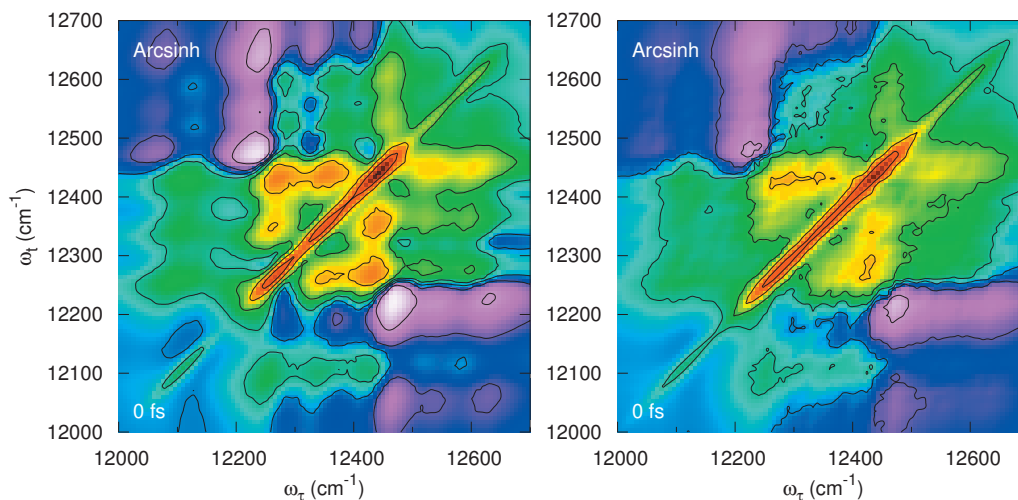
FIG. 4. 2D PE spectra of the FMO model, calculated with very weak optical dephasing $\xi_{ig}=5$ cm^{-1} and inclusion of inhomogeneous broadening, for population time $T=0$. $\delta_{\mathrm{inhom}}=0.5$ in the left panel and 0.7 in the right panel. The spectra are displayed with arcsinh scaling to enhance weaker aspects of the peak profiles.

(right panel). Inclusion of inhomogeneous broadening leads to the averaging of the highly localized diagonal peaks observed in Fig. 2 due to variations of transition frequencies. This leads to an elongation of spectra along the $\omega_\tau=\omega_t$ line, as well as a loss of intensity and poor resolution of the cross peaks. In agreement with the experimental results of Ref. 19, only two peaks can be well resolved along the diagonal. The lower peak corresponds to the spectrally well separated transition to exciton one, while the higher-frequency region represents the contribution from the remaining exciton transitions.

Finally, Fig. 5 shows our best fit of the experimental spectra within the employed simple exciton model. It has been achieved with the optical dephasing rate $\xi_{ig}=30$ cm^{-1}
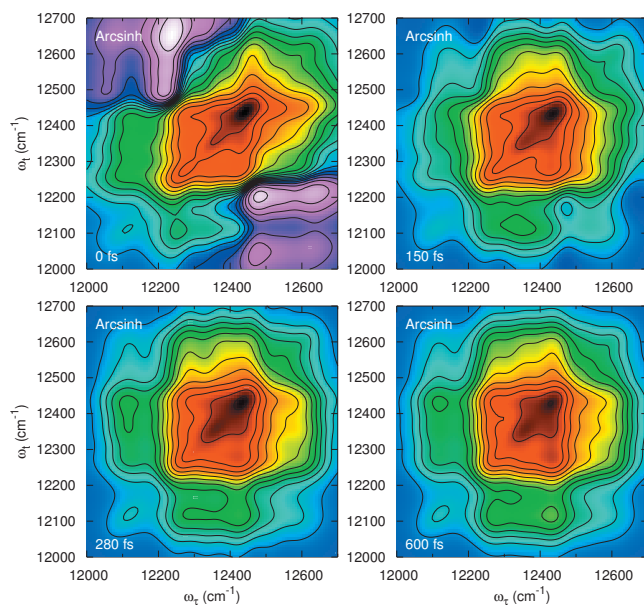

FIG. 5. 2D PE spectra of the FMO model, calculated with $\xi_{ig}=30$ cm^{-1} and $\delta_{\mathrm{inhom}}=0.5$ for various population times as indicated. The spectra are displayed with arcsinh scaling to enhance weaker aspects of the peak profiles. The figure shows the best reproduction of the experimental 2D signals of Ref. 19.

and $\delta_{\mathrm{inhom}}=0.5$. As in Ref. 19, the signals for four values of the population time $T=0$, 150, 280, and 600 fs are shown. Since ESA is not included, the simulated signals miss the negative contribution in the region $\omega_t > \omega_\tau$ (above the diagonal). Otherwise, the agreement with experimental profiles is satisfactory. For larger T, population relaxation leads to an intensity redistribution between the cross peaks.[38] The development of a strong and broad peak below the diagonal with increasing T is a typical experimental observation[19,20] and has also been reproduced in previous simulations.[23] This finding is easy to rationalize. Since population relaxation progresses with T, emission occurs at lower frequencies as T increases. The analysis of coherent oscillations in peak intensities is slightly more involved. In the next section the intensity evolution of individual peaks is considered in more detail.

Before closing this section, we briefly address the effect of a stronger exciton dephasing rate ξ_{ij} on the 2D profiles. It can only become prominent at larger population times (cf. Fig. 1), since the dephasing becomes more efficient with T. Since dephasing rates scale with the difference in energy between two states, optical dephasing, ξ_{ig}, should always be stronger than the dephasing between excited states, ξ_{ij}. The effect on spectra of stronger ξ_{ij} (5 cm^{-1}, left panel and 20 cm^{-1}, right panel) for a fixed value of the optical dephasing ($\xi_{ig}=35$ cm^{-1}) is shown in Fig. 6. As can be seen, the spectral profiles are not strongly influenced by the dephasing rate. Overall peak widths and intensities are relatively unaffected. Since the dephasing between excited states does not significantly alter 2D spectra snapshots, a record of intensity evolution of a particular peak is required to gain information about the decoherence time scale.

C. Peak-specific evolution of 2D signals

In Ref. 19, the intensities of the lowest diagonal peak (DP 1–1) and of the lower ($\omega_t < \omega_\tau$) cross peak between excitons one and three (CP 1–3) were measured as a function of the population time, T. The intensities of the peaks exhibited
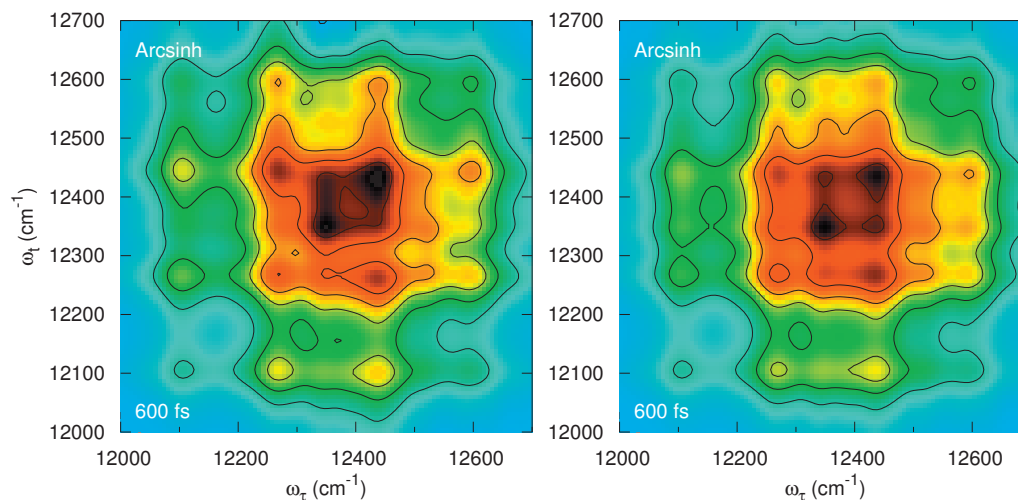
FIG. 6. 2D PE spectra of the FMO model, calculated with optical dephasing $\xi_{ig}=35$ cm, without inhomogeneous broadening, and for the population time $T=600$ fs. The exciton coherence dephasing is $\xi_{ij}=5$ cm^{-1} (left panel) and 20 cm^{-1} (right panel). The spectra are displayed with arcsinh scaling to enhance weaker aspects of the peak profiles.

strong quantum beating with multiple frequencies for at least 660 fs. The oscillations were attributed to electronic coherences between excitons. Furthermore, it has been argued that so-called coherence transfer takes place; the observed multiple frequencies in the intensity evolution of CP 1–3 were assigned to the frequencies between all participating exciton transitions.

This interpretation suggests that the bath induces transfer between the excitonic coherences (ρ_{ij}), and simultaneously allows the coherences to survive on an experimentally observable time scale. The model employed in the present work does not include coherence transfer mediated by the bath, but it provides an estimate of coherence lifetimes in the presence of several dephasing mechanisms directly from experimental observables. Note that in the existing simulations of conceptually new 2D spectroscopies for the FMO complex[26,27] exciton dephasing has not been taken into account.

In the absence of dissipation, cross peaks are expected to oscillate with T like the corresponding off-diagonal $\rho_{ij}(t)$ elements of the reduced density matrix, i.e., with a frequency equal to the energy difference between corresponding excitons.[24,39] The decay of the oscillations is induced by dissipation. While the coherences of the density matrix decay with the rates ξ_{ij}, the intensity modulations of the cross peaks can be further influenced by the optical dephasing (ξ_{ig}) and inhomogeneous broadening.

As in the reported experiment,[19] we focus on CP 1–3 located at $\omega_t=E_1=12101$ cm^{-1}, $\omega_\tau=E_3=12346$ cm^{-1} as well as on DP 1–1 at $\omega_t=\omega_\tau=12101$ cm^{-1}. The calculated intensities of CP 1–3 and DP 1–1 with respect to the population time are shown in Figs. 7 and 8, respectively (a 10 fs population time step was employed in the calculations). The dotted line in Fig. 7(a) corresponds to the idealized case of Fig. 2, i.e., to the limit of very weak dephasing, $\xi_{ig}=\xi_{ij}=5$ cm^{-1}, and no inhomogeneous broadening, $\delta_{\text{inhom}}=0$. In this limit, a well-resolved long-lived oscillation in the intensity of CP 1–3 with a period of 136 fs (determined by the energy difference between excitons three and one, $E_3-E_1=245$ cm^{-1}) is observed. While an increase in optical

dephasing considerably influences the 2D spectral profiles (Fig. 3), it does not significantly dampen the oscillations in the cross peak intensity. The dashed and solid lines in Fig. 7(a) have been obtained with $\xi_{ig}=20$ cm^{-1} and $\xi_{ig}=35$ cm^{-1}, respectively ($\xi_{13}=5$ cm^{-1} has been retained).

To demonstrate how cross-peak intensity oscillations map the corresponding off-diagonal density matrix elements, Fig. 7(b) shows the evolution of CP 1–3 for $\xi_{13}=5$ cm^{-1} (solid line) and $\xi_{13}=20$ cm^{-1} (dashed line). Since the
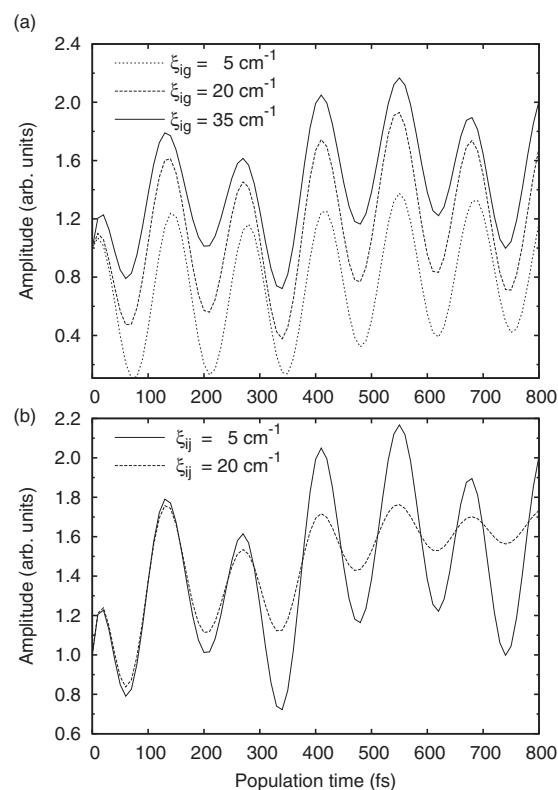

FIG. 7. The normalized amplitude of CP 1–3 as a function of population time, for (a) various values of the optical dephasing ξ_{ig} and $\xi_{ij}=5$ cm^{-1}, and (b) various values of the dephasing rate ξ_{ij} with $\xi_{ig}=35$ cm^{-1}. The solid lines in (a) and (b) represent the same data.

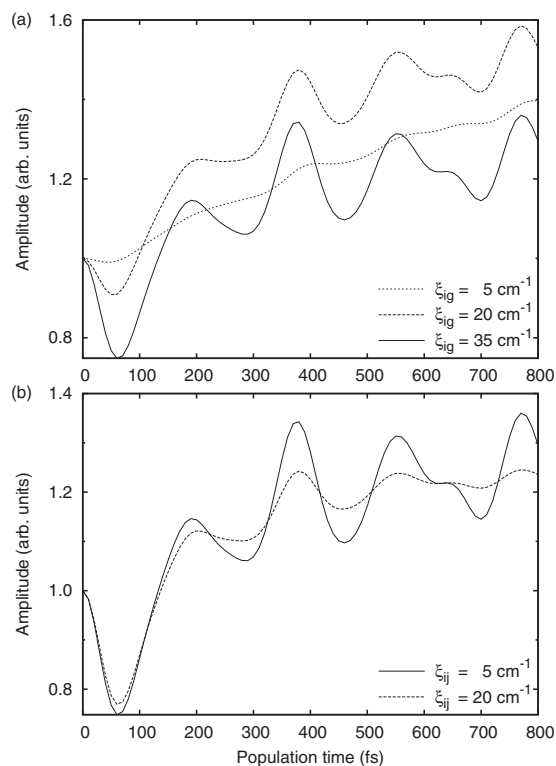FIG. 8. The normalized amplitude of DP 1–1 as a function of population time, for (a) various values of the optical dephasing ξ_{ig} and $\xi_{ij}=5$ cm^{-1}, and (b) for various values of the dephasing rate ξ_{ij} with $\xi_{ig}=35$ cm^{-1}. The solid lines in (a) and (b) represent the same data.
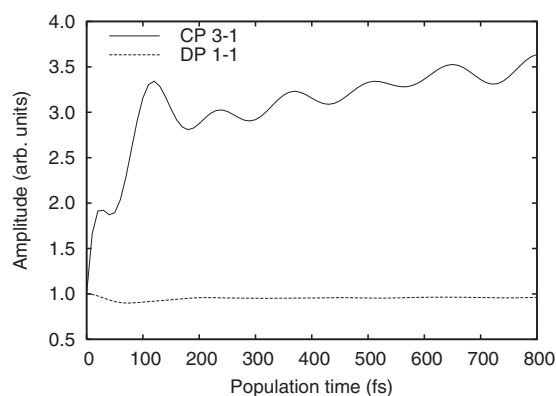

FIG. 9. The normalized amplitude of CP 1–3 and DP 1–1 as a function of population time using parameters that best reproduce the experimental 2D spectra: $\xi_{ig}=30$ cm^{-1} and $\delta_{\text{inhom}}=0.5$ (cf. Fig. 5). A weak dephasing, $\xi_{ij}=5$ cm^{-1}, is used.

strength of the dephasing scales with the energy difference between states, a value for the optical dephasing ξ_{ig} $=35$ cm^{-1} is used. As can be seen, the decay of the cross peak oscillation is determined by the dephasing between exciton states, ξ_{13}, in the same manner as the decay of $\rho_{13}(t)$ in Fig. 1(b). Comparing with experimental results,[19] a moderate value of the dephasing rate, $\xi_{13}=20$ cm^{-1} or weaker, must be used in order to resolve oscillations beyond 660 fs.

The intensity of DP 1–1 [Fig. 8(a), dotted line] exhibits very weak oscillations when idealistic values for dephasing ($\xi_{ig}=\xi_{ij}=5$ cm^{-1}) and inhomogeneous broadening (δ_{inhom} $=0$) are used. As can be seen in Fig. 8(a), an increase in optical dephasing induces oscillations in the diagonal peak. This effect scales with the strength of the optical dephasing and can be understood by comparing 2D spectra in the ideal case (Fig. 2) and in the case of stronger optical dephasing (Fig. 3). The modulation is most likely due to the spread of peak widths, which leads to the overlap of the oscillating cross peaks with the diagonal peaks. In the specific case of DP 1–1, the oscillation can be approximated to be 223 cm^{-1} (corresponding to a period of ≈ 150 fs), which is approximately equal to the energy difference between excitons one and two ($E_1=12101$ cm^{-1} and $E_2=12265$ cm^{-1}). As can be seen in the left panel of Fig. 3, the cross peaks between excitons one and two have spread to such an extent that they overlap with DP 1–1. This interpretation is confirmed by Fig. 8(b). Modulations in the amplitude of DP 1–1 observed for $\xi_{ij}=5$ cm^{-1} and $\xi_{ig}=35$ cm^{-1} (solid line) decay faster with an increase in dephasing between the exciton states ($\xi_{ij}=20$ cm^{-1}, dashed line), since this damps the contribut-

ing cross peak oscillations more efficiently. Another source of the oscillations of the diagonal peak intensity is the so-called nonrephasing contribution,[25] which is automatically taken into account in the present calculations.

So far, we did not include the effect of the inhomogeneous broadening on the peak intensity modulations with population time. The best reproduction of the experimental 2D spectra[19] (cf. Fig. 5) is obtained with the adjustable parameters of $\xi_{ig}=30$ cm^{-1} and $\delta_{\text{inhom}}=0.5$. In this case, we find that the coherent modulation of CP 1–3 is reduced and that of DP 1–1 cannot be resolved, even in the case of slow dephasing ($\xi_{ij}=5$ cm^{-1}), as can be seen in Fig. 9. This finding indicates that the signatures of excitonic coherences are rather sensitive to inhomogeneous dephasing.

In the reported experiment both CP 1–3 and DP 1–1 are found to oscillate with multiple frequencies.[19] Within the model employed in this study, each cross peak at a particular $\omega_t=E_i$, $\omega_\tau=E_j$ is expected to oscillate with a single frequency determined by the energy difference $|E_i-E_j|$. The additional frequencies in CP 1–3 (found experimentally[19]) could arise due to the overlap of broadened neighboring peaks. The effects of broad cross peaks on diagonal peaks are observed here, yet they are insufficient to produce additional oscillations in either diagonal or cross peak intensities. This result strongly suggests that another physical mechanism must be involved. A possible hypothesis is that the bath initiates a very fast coherence transfer so that the evolution of each off-diagonal element of the system density matrix depends on several frequencies $|E_i-E_j|$. So far, this has not been theoretically confirmed, although a number of developments have recently emerged.[35,40] Another possibility is that high-frequency vibrational degrees of freedom of the monomers are excited in the experiment, which give rise to the observed oscillations.

IV. CONCLUSIONS

In this work, we have performed simulations of 2D signals using the model of Ref. 23, which has been extended to explicitly consider the evolution of exciton coherences. Using the EOM-PMA, 2D PE spectra of a single subunit of the FMO complex were simulated. Realistic pulse durations

were considered and pulse-overlap effects were taken into account. The simulations reproduce peak profiles and allow to reveal both diagonal and cross peak oscillations, the latter being visual representations of quantum coherences.

We have thoroughly studied the effects of various dephasing mechanisms on the exciton dynamics, 2D profiles, and oscillations in peak intensity with population time within the Redfield equation model. We have identified the broadening parameters that result in 2D spectra that are in agreement with experimental results.[19] The evolution of 2D spectra with population time is adequately reproduced apart from the negative contribution due to ESA.

Multiple frequencies in peak oscillations, as detected experimentally, were not observed in the simulations. Since the secular approximation has been employed for the description of the system-bath interaction, the phenomenon of coherence transfer through dissipation could not be addressed. The conclusion can be drawn that the fast oscillations of cross peaks observed in experimental data must arise from a more complicated interaction between excitons and (bath) vibrations than is considered here. Consequently, further developments in the description of the mechanisms underlying energy transfer in the FMO complex are required. A dynamical description beyond the Redfield and Förster theories has been recently proposed.[35] It allows for long-lived coherences, but coherence transfer could not be addressed in the dimer model studied.

Resonance Raman experiments[41–43] have revealed dozens of BChl vibrational modes with frequencies in the range from 88 to 1700 cm^{-1}. These and lower-frequency vibrations have been resolved in a recent fluorescence line-narrowing experiment[44] on the FMO complex of *Cb. tepidum*. The most intense bands lie in the regions near 200, 770, 1200, and 1600 cm^{-1} and are close to the frequencies obtained by a Fourier transform of the experimental 2D peak oscillations with population time.[19] As has been shown theoretically[29,39] and experimentally,[45] the dynamics of vibrational modes can considerably alter the 2D peak profiles and coherent vibrational motion can contribute to peak intensity oscillations.[39] A study of the effect of damped intramonomer high-frequency vibrational modes on the 2D signals of the FMO complex is a challenging problem, which is currently under investigation.

ACKNOWLEDGMENTS

[1] R. Blankenship, *Molecular Mechanisms of Photosynthesis* (Blackwell Science, Oxford, 2002).
[2] T. Renger, V. May, and O. Kühn, Phys. Rep. **343**, 137 (2001).
[3] H. van Amerongen, L. Valkunas, and R. van Grondelle, *Photosynthetic Excitons* (World Scientific, Singapore, 2000).
[4] G. McDermott, S. M. Prince, A. A. Freer, A. M. Hawthornthwaite-Lawless, M. Z. Papiz, R. J. Cogdll, and N. W. Isaacs, Nature (London) **374**, 517 (1995).
[5] J. Koepke, X. Hu, C. Muenke, K. Schulten, and H. Michel, Structure (London) **4**, 581 (1996).
[6] W. Kühlbrandt, D. N. Wang, and Y. Fujiyoshi, Nature (London) **367**, 614 (1994).
[7] R. E. Fenna and B. C. Matthews, Nature (London) **258**, 573 (1975).
[8] S. G. Johnson and G. J. Small, Chem. Phys. Lett. **155**, 371 (1989).
[9] S. G. Johnson and G. J. Small, J. Phys. Chem. **95**, 471 (1991).
[10] E. M. Franken, S. Neerken, R. J. W. Louwe, J. Amesz, and T. J. Aartsma, Biochemistry **37**, 5046 (1998).
[11] S. Savikhin and W. S. Struve, Biochemistry **33**, 11200 (1994).
[12] S. Savikhin and W. S. Struve, Photosynth. Res. **48**, 271 (1996).
[13] V. Gulbinas, L. Valkunas, D. Kuciauskas, E. Katilius, V. Liuolia, W. Zhou, and R. E. Blankenship, J. Phys. Chem. **100**, 17950 (1996).
[14] A. Freiberg, S. Lin, K. Timpmann, and R. E. Blankenship, J. Phys. Chem. B **101**, 7211 (1997).
[15] S. I. E. Vulto, A. M. Streltsov, and T. J. Aartsma, J. Phys. Chem. B **101**, 4845 (1997).
[16] S. I. E. Vulto, S. Neerken, R. J. W. Louwe, M. A. de Baat, J. Amesz, and T. J. Aartsma, J. Phys. Chem. B **102**, 10630 (1998).
[17] S. Savikhin, D. R. Buck, and W. S. Struve, J. Phys. Chem. B **102**, 5556 (1998).
[18] R. J. W. Louwe and T. J. Aartsma, J. Phys. Chem. B **101**, 7221 (1997).
[19] G. S. Engel, T. R. Calhoun, E. L. Read, T.-K. Ahn, T. Mančal, Y.-C. Cheng, R. Blankenship, and G. R. Fleming, Nature (London) **446**, 782 (2007).
[20] T. Brixner, J. Stenger, H. M. Vaswani, M. Cho, R. E. Blankenship, and G. R. Fleming, Nature (London) **434**, 625 (2005).
[21] T. Renger and V. May, J. Phys. Chem. A **102**, 4381 (1998).
[22] S. I. E. Vulto, M. A. de Baat, S. Neerken, F. K. Nowak, H. van Amerongen, J. Amesz, and T. J. Aartsma, J. Phys. Chem. B **103**, 8153 (1999).
[23] M. Cho, H. M. Vaswani, T. Brixner, J. Stenger, and G. R. Fleming, J. Phys. Chem. B **109**, 10542 (2005).
[24] Y.-C. Cheng, G. S. Engel, and G. R. Fleming, Chem. Phys. **341**, 285 (2007).
[25] Y.-C. Cheng and G. R. Fleming, J. Phys. Chem. A **112**, 4254 (2008).
[26] D. Abramavicius, D. Voronine, and S. Mukamel, Biophys. J. **94**, 3613 (2008).
[27] D. Voronine, D. Abramavicius, and S. Mukamel, Biophys. J. **95**, 4896 (2008).
[28] M. F. Gelin, D. Egorova, and W. Domcke, J. Chem. Phys. **123**, 164112 (2005).
[29] D. Egorova, M. F. Gelin, and W. Domcke, J. Chem. Phys. **126**, 074314 (2007).
[30] M. F. Gelin, D. Egorova, and W. Domcke, Acc. Chem. Res. **42**, 1290 (2009).
[31] A. Ishizaki and G. R. Fleming, J. Chem. Phys. **130**, 234110 (2009).
[32] S. I. E. Vulto, M. A. de Baat, R. J. W. Louwe, H. P. Permentier, T. Neef, M. Miller, H. van Amerongen, J. Amesz, and T. J. Aartsma, J. Phys. Chem. B **102**, 9577 (1998).
[33] J. Adolphs, T. Renger, and V. May, Biophys. J. **91**, 2778 (2006).
[34] F. Müh, M. E.-A. Madjet, J. Adolphs, A. Abdurahman, B. Rabenstein, H. Ishikita, E.-W. Knapp, and T. Renger, Proc. Natl. Acad. Sci. U.S.A. **104**, 16862 (2007).
[35] A. Ishizaki and G. R. Fleming, J. Chem. Phys. **130**, 234111 (2009).
[36] T. Mančal, A. V. Pisliakov, and G. R. Fleming, J. Chem. Phys. **124**, 234504 (2006).
[37] S. Mukamel, *Principles of Nonlinear Optical Spectroscopy* (University, Oxford, 1995).
[38] A. V. Pisliakov, T. Mančal, and G. R. Fleming, J. Chem. Phys. **124**, 234505 (2006).
[39] D. Egorova, Chem. Phys. **347**, 166 (2008).
[40] P. Rebentrost, M. Mohseni, and A. Aspuru-Guzik, J. Phys. Chem. B **113**, 9942 (2009).
[41] M. Lutz, A. J. Hoff, and L. Brehamet, Biochim. Biophys. Acta **679**, 331 (1981).
[42] J. R. Diers and D. F. Bocian, J. Am. Chem. Soc. **117**, 6629 (1995).
[43] V. Zazubovich, I. Tibe, and G. J. Small, J. Phys. Chem. B **105**, 12410 (2001).
[44] M. Rätsep and A. Freiberg, J. Lumin. **127**, 251 (2007).
[45] A. Nemeth, F. Milota, T. Mancal, V. Lukes, H. F. Kaufmann, and J. Sperling, Chem. Phys. Lett. **459**, 94 (2008).